

## Methodology of Testing for Aluminium Honeycomb Impact Attenuator in Quasi-Static Conditions and Influence of Supporting Structures

Jan Tracz<sup>1,2</sup>, Witold Rządłowki<sup>1</sup>, Tadeusz Majewski<sup>3</sup>, Marco A. Meraz Melo<sup>3</sup>, Adam Cisowski<sup>1</sup>, Krzysztof Zawisliński<sup>1</sup>, Dawid Urbański<sup>1</sup>, Aleksy Figurski<sup>1</sup>, Edyta Ładyżyńska<sup>2</sup>

<sup>1</sup> Institute of Aeronautics and Applied Mechanics, Warsaw University of Technology, ul. Nowowiejska 24, 00-665 Warsaw, Poland

<sup>2</sup> Institute of Micromechanics and Photonics, Warsaw University of Technology, ul. Św. Andrzeja Boboli 8, 02-525, Warsaw, Poland

<sup>3</sup> Instituto Tecnológico de Puebla, Del Tecnológico 420, Corredor Industrial la Ciénega, 72220 Heroica Puebla de Zaragoza, Mexico

\* Corresponding author's e-mail: [jan.tracz.dokt@pw.edu.pl](mailto:jan.tracz.dokt@pw.edu.pl)

### ABSTRACT

This paper examines the influence of two different supports, i.e., composite and steel, on the results obtained during a quasi-static crush test of an aluminum alloy honeycomb impact attenuator. It's part of a vehicle that competes in the Formula Student series and requires safety tests to be eligible to participate in events. The attenuator is tested in two configurations – first with a rigid steel support base and second – with a composite support base, which represents a realistic replica of the first 50 mm of carbon fiber monocoque used in a vehicle. The composite base is less stiff and must be tested with the impact attenuator as it is a possible safety weak point. The testing machine was an Instron 8516 set to a 60 mm/min feed speed with a sampling rate of 1 kHz. The results showed that the values of energy absorbed were higher (7983.9 J to 8732.1 J) for the case with a composite base support, whereas the average forces were similar (about 50 kN). This suggests that a more realistic scenario allows for a higher safety margin rather than a decrease in it. The recommendation is to address the possible energy cumulation as elastic deformation (spring-back effect), which might be unwanted. Further studies could include dynamic testing and other attenuator designs.

**Keywords:** impact attenuators, aluminum alloy honeycomb, quasistatic, impact engineering, FSAE.

### INTRODUCTION

Impact attenuators are crucial to the driver's safety in case of an accident [1]. Their purpose is to prevent the occurrence of high decelerations on a driver by absorbing the kinetic energy of a vehicle in case of a collision. The concept of impact attenuators is widely used in the automotive industry as crumple zones developed in 1952 by Béla Barényi [2]. It is one of many passive safety systems used to improve vehicular

safety. They can be implemented at various parts of the vehicles to diminish the acceleration values resulting from a collision at a given angle and direction and to prevent the main-frame body deformation. Similar concepts are used across various structures e.g. aircrafts [3], [4]. In this paper methods of testing such devices and influences caused by the base supports on the obtained results will be investigated.

When it comes to impact attenuators for formula student vehicles, a few design concepts are

utilized. One of them is the non-structural nose approach. It is a solution where the nose cone and impact attenuator are two separate devices. This comes with a few crucial benefits. In case of a minor incident, the only thing that needs replacement is the nose cone, which is cheap to make as it doesn't require a complicated technological process. This kind of approach was implemented by [5], where the impact attenuator has been made from Rohacell foam. Yet another approach was implemented by [6] where multiple sheets of metal were joined together, and the energy absorption was achieved by plastic deformation of the sheets. More technologically advanced solutions include 3D printed lattices made using 3D printing technology such as the ones presented in [7–10] and [11].

The structural nose can be more challenging. It can be seen in [12] where the designers combined the nose cone and impact attenuator into one device that has been made from bent sheets of aluminum alloy that were welded together. Also, finite element methods were used during the design and after validation to improve the model. However, possibly the most popular solution is to use commercially available honeycomb blocks. They can be arranged into a pyramid model such as one from [13] if it is required (due to space limitations) or just simply an extruded block glued to the anti-intrusion plate. This is a time-effective solution as the required design steps are straightforward and, therefore, used by numerous teams [14–17]. More on aluminum impact attenuator designs have been stored in the reviews [18, 19].

All the designs must be tested. The guidelines dictate the minimum dimensions of the device, the maximum accelerations that can occur, and the minimum energy absorbed necessary to approve the impact attenuator. The test can be dynamic or quasistatic depending on the type of attenuator. The different tests apply to composite structural noses, which shortcut the loading path by using not the anti-intrusion plate but the bulkhead of the chassis. Despite the differences in the design of the impact structures, the chassis supporting it can only be made from composite panels (usually carbon fiber with aluminum alloy honeycomb core) or from steel alloys – a steel space frame [20].

In the case of a tubular space frame chassis, the front part of a vehicle is not tested (the part behind the impact attenuator), but there is a static equivalency spreadsheet where the structure

is evaluated based on the provided mechanical properties of the steel tubes that create the structure. It should be a good approximation as the steel behavior is easy to predict, and finite element analysis showed that the buckling of the chassis is acceptable with an impact attenuator [21]. Some teams, however, develop a composite monocoque, so they must change the testing procedure of the impact attenuator by manufacturing the 50 mm+ replica of the frontal part of a monocoque and testing it all together. This means a more realistic testing scenario enables the test of the anti-intrusion plate (AIP) mounting points yet significantly increases costs.

The whole research is a result of a change in regulations. Until recently, the safety requirements did not state what kind of support structure to put underneath the impact attenuator during the test. Therefore, the safety device was tested on solid steel support, similar to the geometry of a vehicle chassis, yet with much higher stiffness. However, the regulations changed, and it was now mandatory to develop a replica of a frontal part of a chassis if it was a composite monocoque.

The problem addressed in this research is the methodology of calculating the results of energy absorbed by the impact attenuator device in quasi-static tests. The current method calculates the integral from the recorded force as a function of displacement using the midpoint rule. Force is recorded until the energy absorber (in this case, an aluminum alloy honeycomb block) becomes solid, and the force rises sharply. Then, the energy is calculated in the bounds between minimum and maximum displacement. However, this means that the energy absorbed due to compliance (elasticity) is also included in the result.

The goal is to answer the question of whether there will be a difference as a result of using different support structures and what the influence of testing with such a method can be on the results obtained. The collected data will be calculated to obtain important parameters for impact attenuator tests and compliance with rules.

## MATERIALS AND METHODS

The design approach used in the vehicle was a nonstructural nose cone with an impact attenuator located inside the shell body (Figure 1).

This was done due to time and resource constraints but also due to fear of possible accidental



**Figure 1.** Front of the vehicle with nose cone and front wing

damage of the attenuator in transport had it been made as one structural part. The computer-aided design (CAD) view of the frontal part can be seen in Figure 2, together with the frontal wing and its mounting bracket. The wing will be neglected in the crush scenario since it is mounted with M6 bolts and is optimized to have strength and stiffness in the vertical direction, collinear with produced aerodynamical downforce.

The impact attenuator used was one of the most popular solutions, i.e., the aluminum alloy honeycomb block. It had to meet the rules [22] that are summarized in Table 1.

Those assumptions allowed to choose the crush block from the commercially available set offered by the company Plascore [23]. The 5052-aluminum alloy block with a foil gauge of 0.054 mm (0.002 inches) and cell size of 4.7625 mm (3/16 inch) seemed to be the best option (PACL-XR1-5.7-3/16-20-P-5052). Its density is 91.31 kg/m<sup>3</sup>, meaning the whole block weighs about 0.36 kg. Relevant mechanical properties can be seen in Table 2, and additional ones can be found on the manufacturer’s website.

### Test setup

An illustrative example of the setup of the test can be seen in Figure 3. The crush plates are made of 8mm thick steel pieces that are welded together, forming a T-shaped structure. The sticking piece allows for clamping the crush plates in the jaws of the strength testing machine, in this case, Instron 8516. The tested impact attenuator is mounted on the AIP and is a single piece. The investigated base supports are placed between the

**Table 1.** Regulations for an impact attenuator requirements and physical properties

Parameter	Value
Height [mm] <sup>a)</sup>	200
Width [mm]	200
Length [mm]	100
Min test length [mm]	150
Min energy dissipation [J]	7350
Max peak acceleration [g] <sup>a)</sup>	40
Max average acceleration [g] <sup>b)</sup>	20

**Note:** <sup>a)</sup> which is 120 kN of static force assuming 300 kg vehicle; <sup>b)</sup> which is 60 kN of static force assuming 300 kg vehicle.

**Table 2.** Properties of the tested aluminum alloy honeycomb core

Parameter	Value
Height [mm]	200
Width [mm]	200
Length [mm]	100
Crush strength [MPa]	2.62
Crush stroke [mm] <sup>a)</sup>	140 (70%)
Density [kg/m <sup>3</sup> ]	91.31

lower crush plate and the AIP. Once fixed, the machine is set to 60 mm/min feed with a data sampling rate of 1 kHz. The bases are placed between Anti-intrusion plate and lower crush plate. The test machine, bolt holes, etc., are not depicted.

### Base support – steel

The first setup contains a steel support base under the anti-intrusion plate. It is made from four

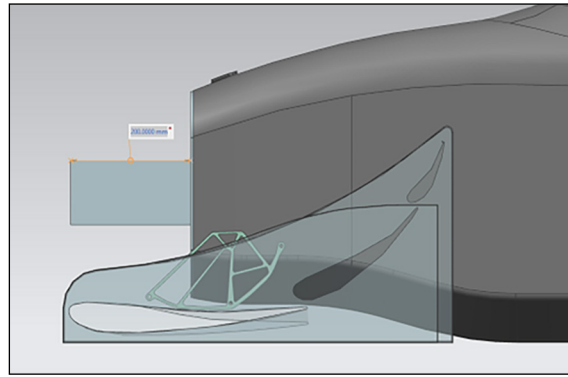


Figure 2. Sectional view of the impact attenuator and the front wing with the mounting bracket

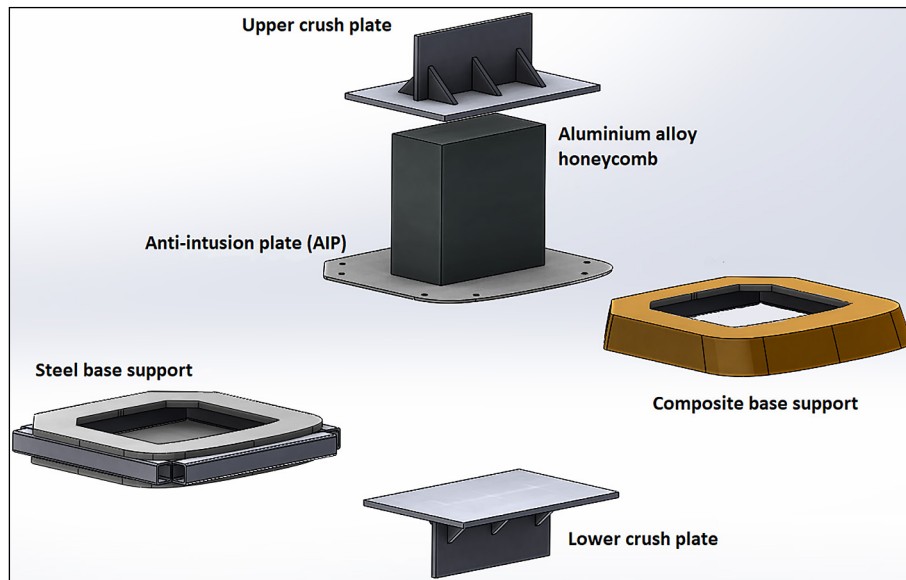


Figure 3. Illustration of the test setup with two tested variants – steel base support and composite one

square 30 mm steel profiles with a wall thickness of 3 mm. The setup is depicted in Figure 4. The square profiles are placed on the outside of the anti-intrusion plate perimeter supporting only the edges. The anti-intrusion plate is mounted to the support with M8 bolts that go through the profiles and crushing plates, and everything is clamped together.

#### Base support – composite replica

The second test setup contains a base that is a 1:1 replica of the first 50 mm of the composite monocoque. It was manufactured using the same process as the carbon fiber chassis. The whole manufacturing process has been documented in other work [25], but there are other options available [26–30]; thus, it can be assumed to be a good representative of an average monocoque design. The test setup is depicted in Figure 5, and it is almost the same as in the case of steel support,

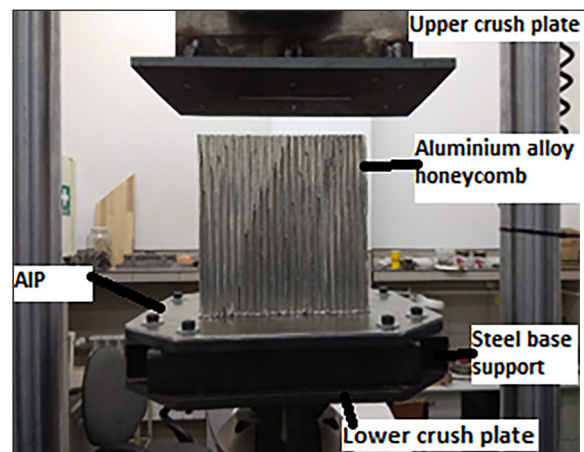


Figure 4. Test setup for steel base support

but due to the slight taper of the replica, an additional plate had to be inserted under the composite base as one of the sides was hanging freely. It has been manufactured using commercially

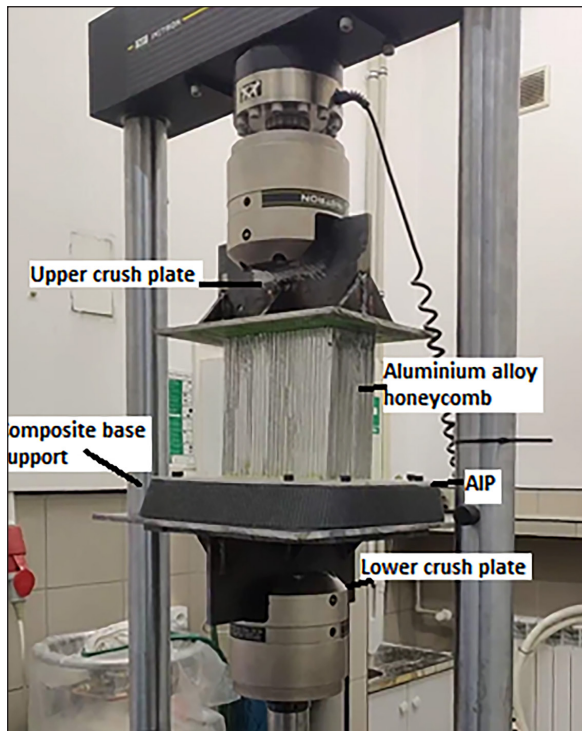


Figure 5. Test setup for the composite base support

available pre-impregnated carbon fiber XPREG 210 [31] and aluminum honeycomb core [32]. The structure is based on a composite panel. The one on the top has a 6 mm thick upper skin with a 10 mm core and 2 mm bottom skin. The core thickness is 10 mm for the whole structure. It can be assumed that its stiffness is lower than that of the steel counterpart by at least an order of one

magnitude due to material and geometrical properties. In both cases, epoxy adhesive was used to bond the honeycomb block to the aluminum alloy AIP plate. The honeycomb comes pre-crushed from one side by the manufacturer for this purpose so that the surface area is the largest. The adhesive used was epoxy adhesive EA3425 as in [33], and the surface was prepared similarly to T4 treatment from [34].

## RESULTS

The test results can be seen in Figure 6. The data was recorded until the force began to rise, which means that the crushing stroke of the block was reached, and there was no more material to absorb the energy, i.e., the block was pressed into a solid. The obtained data must be processed to calculate absorbed energy and maximum forces relevant for comparing the two methods. Additionally, the resulting acceleration values were calculated assuming the vehicle’s mass would be 300 kg and expressed as a multiplicity of gravitational acceleration, which is a common way to present such results.

### Energy absorbed and forces

The energy absorbed can be assumed to be the area under the graph. It was calculated in the bounds between zero and maximum displacement

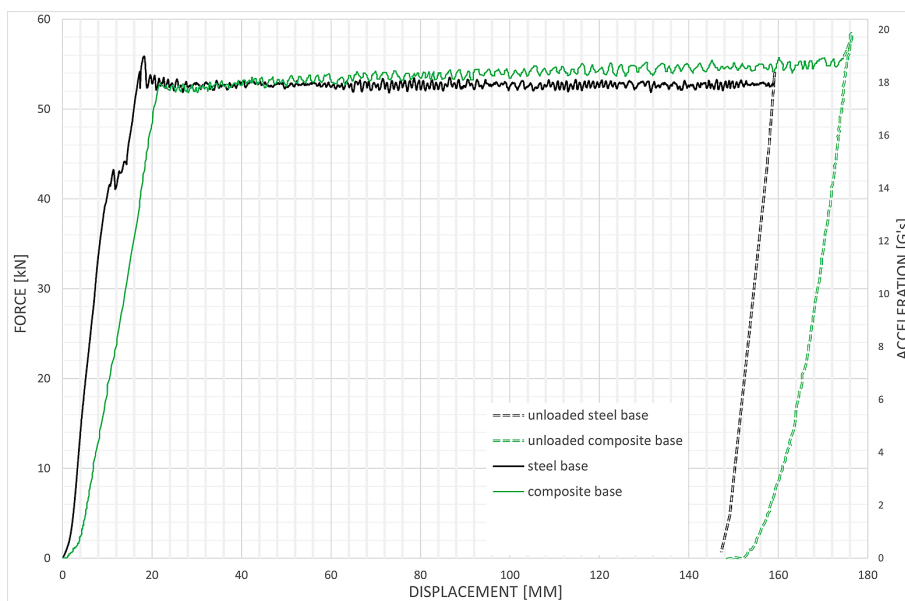


Figure 6. Force and resulting acceleration as a function of displacement registered during the quasi-static crush tests

as it is required to present this data in safety reports for the impact attenuators. It is calculated as a simple integral using the midpoint rule and summed to obtain the final value of absorbed energy. Pseudocode can be denoted in the way shown in Equation 1.

$$E_i = F_i \times (P_i - P_{i-1}) + E_{i-1} \quad (1)$$

where:  $E_i$  – total energy absorbed at current time step (J),  $F_i$  – force at given time step (kN),  $P_i$  – position of a machine at a given time step (mm),  $P_{i-1}$  – position of the machine at the previous time step (mm),  $E_{i-1}$  – total absorbed energy from previous steps (J).

The original integration method employed was the rectangular (midpoint) rule, as recommended by the regulatory guidelines. To enhance the accuracy of the results, especially given the non-linear nature of the force-displacement curves, the trapezoidal rule was implemented instead. The trapezoidal rule is particularly effective for integrating non-linear functions because it averages the heights at each end of the subinterval, thereby providing a better approximation over each segment. Simpson’s rule was considered but not used due to the non-smooth nature of the curves involved. The formula used for the trapezoidal rule integration is given in Equation 2.

$$E_i = E_{i-1} + \frac{(F_i + F_{i-1})}{2} \times (P_i - P_{i-1}) \quad (2)$$

Despite this change in the integration method, the differences in calculated energies were minimal. For the steel support, using the rectangular rule resulted in an energy absorption of 7983.96 J, compared to 7984.17 J using the trapezoidal rule. For the composite support, the energy absorption figures were 8732.06 J for the rectangular rule and 8721.10 J for the trapezoidal rule. This

variation in the composite support results was primarily due to a notable increase in the force gradient around the 16–20 mm mark of displacement, which can be observed in the Figure 6. The difference of approximately 0.12% is deemed negligible for the overall results.

The average force is calculated as a weighted average. This is because the steps recorded by the machine might not be equal. The weight of each step is the distance traveled by the machine in each time step and is multiplied by the force at a given step. The products of this multiplication are summed, and the resulting outcome is divided by the final position of a test (the n-th value). The formulas for calculating the average force are presented in Equation 3.

$$F_{w\_avg} = \frac{\sum_0^n (F_i \times (P_i - P_{i-1}))}{P_n} \quad (3)$$

where:  $F_{w\_avg}$  – average weighted force (kN),  $P_n$  – final displacement value (mm).

The raw data was processed using the above formulas, and the results are shown in Table 3.

### Energy released and spring-back

Next, what happens after the load is released was also investigated. The interesting behavior was found in the case of composite support, and it is depicted in Figure 7. The springback effect is present, and the structure releases stored energy. Since the test measures both the elastic energy resulting from compliance of the test structure and the plastic energy from crushing the honeycomb core. Therefore, it was decided to calculate the total and net energy absorbed in the test. This will be done by subtracting the energy released during unloading from total energy. The net energy absorbed

**Table 3.** Test results

Parameter	Steel base support	Composite base support
Maximum displacement [mm]	158.9	174.1
Maximum force [N]	55886.3	55714.2
Average weighted force [N]	50264.1	50031.3
Energy absorbed at 150 mm (and at max displacement) [J]	7394 (7983.9)	7516.4 (8732.1)
Spring-back <sup>a)</sup> [mm]	11	28
Maximum acceleration [G's]	18.99	18.93
Average acceleration [G's]	17.08	17

**Note:** <sup>a)</sup> when the compressive force has been brought to zero, this is the distance which the sample traveled back from the maximum displacement value.

for the case of composite support is 8327.9 J (loss of 404.26 J), whereas, for the case of steel support, it was 7711.6 J (loss of 272.4 J).

## DISCUSSION

The results presented in the previous section illustrate notable differences between the two methods. The steel base support demonstrates less compliance than its counterpart, as evidenced by the maximum displacement being 15.2 mm higher for the composite base support, indicating significant additional deflection. The graph depicts a less steep initial elastic region for

the composite base, suggesting lower stiffness compared to the steel base.

Upon visual examination, the steel support showed no permanent deformation, whereas the composite base exhibited slight bending as a result of the test (Figure 8). No visible damage or cracks were observed; however, the potential for microcracks under significant loading forces cannot be dismissed and may be verified through non-destructive testing methods such as ultrasound or acoustic emission [35]. The aluminum alloy anti-intrusion plate underwent permanent deflection, reaching the yield limit by about 2 mm for the steel base and 6 mm for the composite one.

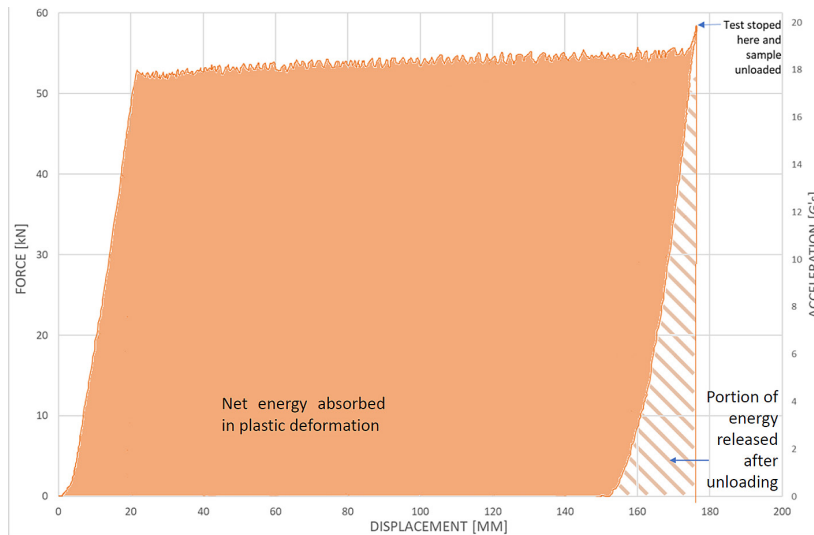


Figure 7. Total and net energy absorbed during the test for composite base support case

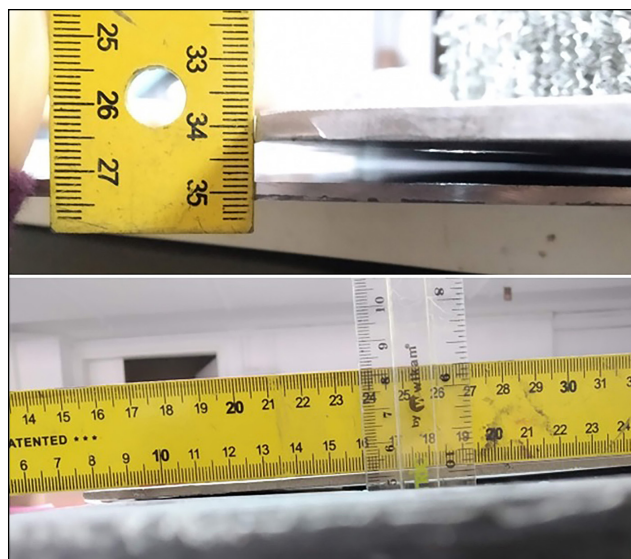


Figure 8. The deflection of the anti-intrusion plate for the case of composite base (top) and a small bend in the composite support found after the test (bottom)

The total energy absorbed was greater for the composite base, largely due to the longer displacement, even though the force values were comparable. Variations in crush strength, which the material manufacturer indicates may fluctuate by up to 10%, could also influence these results. Nonetheless, the consistency in measured average and peak forces suggests that the honeycomb blocks used were of similar quality and from a single batch.

A significant difference in spring-back values – 28 mm for composite versus 11 mm for steel support—mirrors the difference in maximum displacement between the two tests (15.2 mm). This further corroborates that the additional energy absorption is attributable to the structure’s compliance, which stores the energy as potential energy, later released once the load is removed, thus decreasing the final value of energy absorbed. Figure 7 better illustrates this phenomenon, highlighting it prominently for the composite base support case.

Furthermore, we have included a comparison with other studies’ results in the field. The criterion for comparison was that the impact attenuator was made from an aluminum alloy honeycomb. Three studies were chosen [36–38]. The comparison is presented in Table 4.

Factors influencing the results in our study and others in the field are primarily centered on material and design variability. Differences in honeycomb structure, such as cell size or alloy type, significantly affect the energy absorption capabilities and deceleration outcomes. These variances are evident in the differing peak and average decelerations reported across studies. For instance, higher peak decelerations in some studies could be attributed to faster impact speeds or more rigid testing configurations, which alter the dynamics of energy absorption and the mechanical response of the impact attenuators.

Additionally, the deflection of the anti-intrusion plate, especially notable in the composite base with a greater deflection of 6 mm compared to 2 mm in the steel base, indicates a higher energy absorption capacity. This deflection is a critical factor in designing impact attenuators, underscoring the importance of optimizing the attenuator design to balance energy absorption with minimal structural compromise. This approach ensures performance efficacy while managing the physical behaviours of the attenuators under load.

Also, in the study [37] one of the tests showed a considerable difference between crush energy absorbed and the “kinetic” energy. This was also observed in this study as some portion of energy absorbed will be rebound as a result of compliance. The more compliant the design the more energy it will store. This is not ideal as it can lead to designing an impact attenuator that stores energy rather than absorbing it by plastic deformation.

## CONCLUSIONS

The comparative analysis between the composite and steel base supports illustrates that the composite base, offering a more realistic test scenario, exhibits higher energy absorption due to its greater compliance. However, this comes with a significant amount of spring-back – about 16% of the crushed length – which may not be desirable as it extends the negative acceleration period exerted on the driver. Such behavior might not accurately represent real-world scenarios, given the limitations of the quasi-static crush test replicating only the first 50 mm of a composite chassis.

Both test scenarios succeeded in absorbing the requisite energy amounts (over 7350 J), even when considering net energy at the 150 mm mark. Yet, the consideration of energy types – plastic versus elastic deformation – raises questions about the adequacy of current testing standards. It

**Table 4.** Comparison of test results with other studies

Parameter	This study (steel/composite support)	Lufinka A.	Fahland et al.	Coppola et al.
Absorbed energy [J]	7711.6/8327.9	8213	7 072.75	7740
Peak deceleration [G]	18.99/18.93	28.13	19.75	23.01–31.97
Average deceleration [G]	17.08/17.0	11.8	14.8	14.52–18.91
Anti-intrusion plate deflection [mm]	2/6	15	n/d	12.0
Crush length [mm]	147.9/146.5*	n/d	130.5	n/d

**Note:** Calculated as maximum deflection decreased by the spring-back value from Table 3.

might be beneficial to revise testing protocols to differentiate between these energy types, potentially through the inclusion of unloading phases in the test procedures to better mimic real-world dynamics and ensure a focus on energy forms most critical to safety.

Recommendations for regulatory practices should, therefore, specify which types of energy absorption and test parameters are critical, ensuring clarity in competitive educational settings such as Formula SAE. This clarity would aid teams and engineers in designing safer, more compliant vehicles.

Furthermore, the findings suggest potential revisions in vehicle design, particularly the size and weight of impact attenuators, to optimize safety without compromising performance. Further testing is essential to validate whether reduced-size attenuators maintain safety, especially in terms of mitigating spring-back effects, which could influence other safety components like the head and neck support (HANS) device.

Ultimately, these insights could guide improvements in both vehicle safety standards and performance metrics, emphasizing a balance between protective features and competitive performance in educational motorsport settings.

## REFERENCES

- Perz R. Matyjewski M. Risk of experiment failure – analysis of the crash test reliability. *Journal of KONBiN*, 41–48: 1(29),
- Prof. h.c. Béla Barényi online: [http://www.dpma.de/ponline/erfindergalerie/e\\_bio\\_barenyi.html](http://www.dpma.de/ponline/erfindergalerie/e_bio_barenyi.html).
- Deskiewicz A., Perz R. Agricultural aircraft wing slat tolerance for bird strike. *Aircraft Engineering and Aerospace Technology*. 2017; 89(4): 590–598.
- Bielawski R., Rządowski W., Kowalik M., Kłonica M. Safety of aircraft structures in the context of composite element connection, international review of aerospace engineering (IREASE), 2020; 13(5): 159–164, DOI: 10.15866/irease.v13i5.18805.
- Schormans J.M.J. 2010. The design of a formula student front impact attenuator, Eindhoven University of Technology.
- Boria, Simonetta. 2010. Behaviour of an impact attenuator for formula SAE car under dynamic loading. *International Journal of Vehicle Structures & Systems*. 2. 10.4273/ijvss.2.2.01.
- Maskery, I., Aboulkhair, N.T., Aremu, A., Tuck, C., Ashcroft, I., Wildman, R., Hague, R. A mechanical property evaluation of graded density Al-Si10-Mg lattice structures manufactured by selective laser melting. *Mater. Sci. Eng. A* 2016; 670: 264–274.
- Vrána, R., Červinek, O., Maňas, P., Koutný, D., Paloušek, D. Dynamic loading of lattice structure made by selective laser melting-numerical model with substitution of geometrical imperfections. *Materials* 2018; 11, 2129. <https://doi.org/10.3390/ma11112129>
- Moj, K.G. Robak, R. Owsinski, A. Kurek, K. Žak, and D. Przysiężniuk. A new approach for designing cellular structures: design process, manufacturing and structure analysis using a volumetric scanner.” *J. Mech. Sci. Technol.*, Nov. 2022; 36(0): 1–6, <https://doi.org/10.1007/S12206-022-2107-1/METRICS>
- Vrana, R., Koutny, D., Palousek, D. Impact resistance of different types of lattice structures manufactured by slm. *MM Sci. J.* 2016; 2016: 1579–1585.
- Szczesiak, R., Kowalik, M., Cader, M., Pyrzanowski, P. Parametric numerical model for predicting mechanical properties of structures made with FDM technology from polymeric materials. *Polimery*, 2021; 63(9), 626–632. <https://doi.org/10.14314/polimery.2018.9.7>
- Belingardi, G.; Obradovic, J. Design of the impact attenuator for a formula student racing car: Numerical simulation of the impact crash test. *Journal of the Serbian Society for Computational Mechanics*. 2010; 4: 52–65.
- Hart, J., Kennedy, C., LeClerc, T., Pollard, J. *Fsae Impact Attenuator*, WPE, 2010
- Vettorello, A., Campo, G.A., Goldoni, G., Giacalone, M. Numerical-experimental correlation of dynamic test of a honeycomb impact attenuator for a formula SAE vehicle. *Metals*. 2020; 10(5): 652. <https://doi.org/10.3390/met10050652>
- Fahland, Jason & Hoff, Craig & Brelin-Fornari, Janet. Evaluating impact attenuator performance for a formula SAE vehicle. *SAE International Journal of Passenger Cars – Mechanical Systems*. 2011; 4: 836–847. 10.4271/2011-01-1106.
- Sørensen, J.B., Simonsen, C.D., Broberg, N. Modelling and mass optimisation of an aluminium honeycomb impact attenuator, Aalborg University, 2020. Available: [https://projekter.aau.dk/projekter/files/334484255/DMS4\\_Fib14\\_23B.pdf](https://projekter.aau.dk/projekter/files/334484255/DMS4_Fib14_23B.pdf)
- Praveen, M., & Lepšik, P. Design and analysis of honeycomb based impact attenuator. *Manufacturing Technology*. 2020; 20: 639–645. 10.21062/mft.2020.089.
- Quoc, P.M., Krzikalla, D., Mesicek, J., Petru, J., Smiraus, J., Sliva, A., Poruba, Z. On aluminum honeycomb impact attenuator designs for formula student competitions. *Symmetry* 2020; 12: 1647. <https://doi.org/10.3390/sym12101647>
- Naman, A., Janmit, R., Gaurav S. Design and Analysis of Impact Attenuator: A Review. *International*

- Journal of Mechanical Engineering. 2015; 2: 1–7. 10.14445/23488360/IJME-V2I12P101.
20. Bielawski, R., Kowalik, M., Suprynowicz, K., Rządowski, W., Pyrzanowski, P. Investigation of riveted joints of fiberglass composite materials. *Mech Compos Mater* 2016; 52: 199–210. <https://doi.org/10.1007/s11029-016-9573-4>
  21. Oshinibosi, A. Chassis and impact attenuator design for formula student race car, University of Leeds, 2012.
  22. Formula SAE Rules. 2022. available online: <https://fsaeonline.com/cdsweb/gen/DocumentResources.aspx>
  23. Plastcore CrushLite™ available at <https://www.plastcore.com/honeycomb/energy-absorbers/crushlite/>
  24. LOCTITE EA 9466 available: [https://www.henkel-adhesives.com/pl/pl/produkty/structural-adhesives/loctite\\_ea\\_9466.html](https://www.henkel-adhesives.com/pl/pl/produkty/structural-adhesives/loctite_ea_9466.html)
  25. Rządowski, W., Klik, P., Tracz, J., Kowalik, M. Case study of composite chassis manufacturing process using low temperature molds tempered with gradual heat annealing process. *Advances in Science and Technology Research Journal*. 2022; 16(3): 12–21. doi:10.12913/22998624/147368.
  26. Nazarczuk, M., Cader, M., Kowalik, M., Jankowski, M. Proposition of the methodology of the robotised part replication implemented in industry 4.0 paradigm. W: Szewczyk, R., Zieliński, C., Kaliczyńska, M., red. *Automation 2019: Progress in Automation, Robotics and Measurement Techniques*. T. 920. *Advances in Intelligent Systems and Computing*. 2020; 457–472. doi:10.1007/978-3-030-13273-6\_43
  27. Joel, E. Buntine. Design of a carbon fibre monocoque for a Formula SAE racing car, UNSW Canberra at ADFA.
  28. Chad, A., Bruns, B., Hammond J, Lutter J. *Formula SAE Impact Attenuator Testing*, 2010; 35–46.
  29. Hiller, M. Design of a carbon fiber composite monocoque chassis for a formula style vehicle, Lee Honors College, 2020.
  30. Shi, L., Rice, K. Carbon fibre composite monocoque chassis for a formula student race car, Monash Motorsport, 2019.
  31. XC110 210 g 2 × 2 Twill 3k Prepreg Carbon Fibre manufactured by Easy composites Ltd, Stoke-on-Trent, England. 2020, available online: <https://www.easycomposites.co.uk/xc110-210g-22-twill-3k-prepreg-carbon-fibre> (accessed on December 2020).
  32. 3.2mm(1/8”)CellAluminiumHoneycomb <https://www.easycomposites.eu/3mm-aluminium-honeycomb>
  33. Rządowski, W., Jan, T., Adam, C., Kamil, G., Hubert, G., Palka, M., Kowalik, M. Evaluation of bonding gap control methods for an epoxy adhesive joint of carbon fiber tubes and aluminum alloy inserts. *Materials*, 2021; 14, 1–13. <https://doi.org/10.3390/ma14081977>
  34. Kłonica M. Analysis of the effect of selected factors on the strength of adhesive joints. *IOP Conference Series: Materials Science and Engineering*. 2018; 393. DOI 10.1088/1757-899X/393/1/012041.
  35. Skoczylas, J., Kłonica, M., Samborski S. A study on the FRP composite’s matrix damage resistance by means of elastic wave propagation analysis. *Composite Structures*. 2022; 297. DOI 10.1016/j.compstruct.2022.115935
  36. Lufinka, A. 2017. Crash Test of the Student Racing Car Impact Attenuator. In *Proceedings of the 40th International Conference on Modern Development in Management, Economics and Human Resources 1–4*. Czech University of Life Sciences Prague. Available at <https://dspace.tul.cz/handle/15240/31384>
  37. Fahland, J., Hoff, C., Brelin-Fornari, J. Evaluating Impact Attenuator Performance for a Formula SAE Vehicle. *SAE International Journal of Passenger Cars - Mechanical Systems*. 2011; 4: 836–847. 10.4271/2011-01-1106.
  38. Coppola, L., De Marco, B., Niola, V., Sakhnevych, A., Timpone, F. Impact attenuator optimum design for a FSAE racing car by numerical and experimental crash analysis. *Int. J Automot. Technol*. 2020; 21: 1339–1348. <https://doi.org/10.1007/s12239-020-0126-4>